Studying scattering processes with Lippmann-Schwinger equation

Tamás Páhoki
CP4OU3
Eötvös Loránd University
Date of submission: 19th of November 2021

CONTENTS

I. INTRODUCTION

If we want to learn new physics we need to have theories and experiments, too and both of them demand innovation in its field. Nowadays, the leading research areas are mainly focusing on particle and quantum physics whose are good canditates for understanding our world in a deeper level. In some cases the created theoretical background can be applied in other disciplines, too. This is also the case with the Lippmann-Schwinger equation, what is not only able to describe two-body quantum mechanical scattering processes of nucleons, atoms and molecules, but it can be used for seismic scattering processes. For more than two particle's scattering processes need to formalize in other ways, e.g. the three-body problem can be described by the Faddeev equations [1].

We would like to mention one important property of this equation and the theory that based on it. The Lippmann-Schwinger equation is equivalent the time-independent Schrödinger equation for appropriate boundary contiditons. Therefore the equation must be an integral equation, but keep in mind that we do not have boundary conditions [1].

II. THEORETICAL BACKGROUND AND COMPUTATIONAL METHOD

The Lippmann-Schwinger equation follows as

$$R(k,k') = V(k,k') + \frac{2}{\pi}\mathcal{P}\int_0^\infty \mathrm{d}p\,\frac{p^2 V(k',p)R(p,k)}{(k_0^2-p^2)/2\mu}, \tag{1}$$

where R is the *reaction amplitude* or R *matrix*, V is the scattering potential, k, k' the initial and final center of mass frame momenta, $\mathcal{P}$ denotes Cauchy's principal value, k_0 is corresponds to the E energy, $E = k_0^2/2\mu$ and μ is the reduced mass ($\hbar = 1$). In spherically symmetric cases the method for solving the equation is the partial wave analysis [1]. In this theory we use an approximation which uses only of the $l = 0$ partial wave.

If we know the reaction amplitude we can calculate the δ_0 *phase shift* and the $\mathrm{d}\sigma/\mathrm{d}\Omega$ *cross section*.

$$\tan\delta_0 = -2\mu k_0 R(k_0,k_0) \qquad \frac{\mathrm{d}\sigma}{\mathrm{d}\Omega} = \frac{1}{k_0^2}\sin^2\delta_0 \tag{2}$$

Our goal is to compute this quantities with the function of the initial center of mass frame energy E.

A. Implementation

First, we have to eliminate $\mathcal{P}$, in other words, we need to transform the integral in (1) to a numerically computable, non-singular form. We use the following identity which is the eq. (20.28) from [2]

$$\mathcal{P}\int_0^\infty \mathrm{d}k\,\frac{f(k)}{k^2-k_0^2} = \int_0^\infty \mathrm{d}k\,\frac{f(k)-f(k_0)}{k^2-k_0^2}, \tag{3}$$

therefore the Lippmann-Schwinger equation looks like

$$R(k,k') = V(k,k') + \frac{2}{\pi}\int_0^\infty \mathrm{d}p\,\frac{p^2V(k',p)R(p,k) - k_0^2V(k',k_0)R(k_0,k)}{(k_0^2-p^2)/2\mu}. \tag{4}$$

For the numerical computation we need to discretise the equation. We take a grid in k space with N points labelled with j. We rewrite the variables for simpler readability. This means the following renamings: $k_0 \to k_0$, $k' \to k$, $k \to k_0$ and due to the discretisation and the renaming we have to write $\sum_j k_j$ instead of $\int_0^\infty \mathrm{d}p$.

$$R(k,k_0) \approx V(k,k_0) + \frac{2}{\pi}\sum_{j=1}^{N}\frac{k_j^2V(k,k_j)R(k_j,k_0)}{(k_0^2-k_j^2)/2\mu}w_j - \frac{2}{\pi}k_0^2V(k,k_0)R(k_0,k_0)\sum_{j=1}^{N}\frac{1}{(k_0^2-k_j^2)/2\mu}w_j. \tag{5}$$

k_j-s are the integration points and w_j-s are the weights that come from a Gaussian distribution. (Uniform distribution: $w_j = 1\,\forall j$. This would not be as precise as the Gaussian.)

Due to this discretisation we got a linear equation system that needs to be solved. The unknowns are $R(k_j, k_0)$ for $j \in \{1, ..., N\}$ and $R(k_0, k_0)$, so we have $N+1$ of them, same amount of equations needed. We need a grid in k-space with $N+1$ points. The grid will be

$$k_i = \begin{cases} k_j, & \text{if } i = 1, ..., N \\ k_0, & \text{if } i = 0. \end{cases}$$

If we introduce the following notations, $R(k = k_i, k_0) \to R_{i0}$, $V(k = k_i, k_0) \to V_{i0}$, $V(k = k_i, k_j) \to V_{ij}$, the equation system can be written in a simpler way.

$$R_{i0} = V_{i0} + \frac{2}{\pi} \sum_{j=1}^{N} \frac{k_j^2 V_{ij} R_{j0}}{(k_0^2 - k_j^2)/2\mu} w_j - \frac{2}{\pi} k_0^2 V_{i0} R_{00} \sum_{j=1}^{N} \frac{1}{(k_0^2 - k_j^2)/2\mu} w_j. \tag{6}$$

And finally, let's introduce the following vectors to make the equation system to the most compact form.

$$\boldsymbol{R} = \begin{pmatrix} R_{00} \\ R_{10} \\ ... \\ R_{N0} \end{pmatrix}, \quad \boldsymbol{V} = \begin{pmatrix} V_{00} \\ V_{10} \\ ... \\ V_{N0} \end{pmatrix}, \quad \boldsymbol{D} = \begin{pmatrix} D_0 \\ D_1 \\ ... \\ D_N \end{pmatrix}, \quad \text{where} \quad D_i = \begin{cases} +\frac{2}{\pi} \frac{k_i^2 w_i}{(k_0^2 - k_i^2)/2\mu}, & \text{if } i = 1, ..., N \\ -\frac{2}{\pi} \sum_{j=1}^{N} \frac{k_0^2 w_j}{(k_0^2 - k_j^2)/2\mu}, & \text{if } i = 0. \end{cases} \tag{7}$$

With the use of this quanties we can rewrite the discretized form of the original equation (6)

$$\mathbf{F}\boldsymbol{R} = \boldsymbol{V}, \tag{8}$$

where $F_{ij} = \delta_{ij} - D_j V_{ij}$ is the *wave matrix* and δ_{ij} is the Kronecker delta. From the equation (8) the $\boldsymbol{R}$ wave vector can easily be computated (preferably) with a Gauss elimination (or with inverting).

B. Momentum-space potential

As it can be seen in the Lippmann-Schwinger equation, given by (1) we require the momentum-space potential. We can calculate it by using the momentum-space Schrödinger equation, (20.3) of [2]

$$\frac{k^2}{2\mu}\psi(k) + \frac{2}{\pi} \int_0^\infty \mathrm{d}p\, p^2 V(k, p)\psi(p) = E\psi(k), \tag{9}$$

where we are restricted ourselves into the $l = 0$ sector. From this identity the momentum-space potential, (20.4) of [2] takes the following shape

$$V(k, p) = \frac{1}{kp} \int_0^\infty \mathrm{d}r\, \sin(kr) V(r) \sin(pr), \tag{10}$$

where $V(r)$ is the radial potential in the coordinate space.

In the followings we will study 6 different types of potentials, whose coordinate dependent expressions are summarized here.

$$V_{\text{Dirac}}(r) = \frac{\lambda}{2\mu}\delta(r - b) \tag{11}$$

$$V_{\cosh}(r) = -\frac{a}{\cosh^2(r)} \tag{12}$$

$$V_{\exp}(r) = a\mathrm{e}^{-br} \tag{13}$$

$$V_{\text{Gauss}}(r) = a\mathrm{e}^{-b(r-c)^2} \tag{14}$$

$$V_{\text{Yukawa}}(r) = a\frac{\mathrm{e}^{-br}}{r} \tag{15}$$

$$V_{\text{LJ}}(r) = \frac{a}{r^k} - \frac{b}{r^l} \tag{16}$$

Unfortunately, because of the singular behaviour of the Lennard-Jones potential, denoted by V_{LJ}, at $r = 0$ causes the non-existence of the momentum space potential form, therefore it doesn't require further investigation.

C. Computation

We shortly summarize the computational methods that are used for the implementation above the mentioned discretisational thoughtprocess. We used Wolfram Mathematica for calculating the momentum-space potential from (11)-(15). For the numerical calculations we used Python. The momentum-space grid spaced uniformly, so the sampling points are equidistants. But the used w weights are comes from a Gaussian distribution. We chose the mean for 1 for the sake of correct order of magnitude and the standard deviations for 0.5. We used multiple samplings for a given distribution and after that we averaged them for the sake of the simulation's higher precision.

We used 20 random generated weighting (# of measurements) and 50 points in the momentum space grid (# of grid points).

III. RESULTS

In this section we summarize the results for the various potentials with respect to its momentum-space form. We show 3 figures for each scenario. On the first, one can see the tangent of the phase shift calculated from the linear equation system's solution, the $\boldsymbol{R}$ reaction amplitude plugged into (2). The second pictures show the phase shifts and the third ones the cross sections that are calculated by the phase shifts using (2). We want to have a remark here. One can see that the pictures contain errorbars. We calculated the mean and the standard deviation of the values given by the 20 random generated weighting and then we identify the mean to the value of the specific quantity and the standard deviation to the error of it.

A. Delta-shell potential

$$\text{In coordinate space:} \quad V_{\text{Dirac}}(r) = \frac{\lambda}{2\mu}\delta(r-b) \tag{17}$$

$$\text{In momentum space:} \quad V(k,p) = \frac{\lambda}{2\mu}\frac{\sin(kb)\sin(pb)}{kp} \tag{18}$$

We ran the simulation for one value of the parameters because we can easily guess the dependences from them. If we vary b than nothing will change, if $\lambda/2\mu$ is increasing, V will so and therefore R and $\tan\delta_0$ in a linear way but the δ_0 will increase arctan-ly and $\mathrm{d}\sigma/\mathrm{d}\Omega$ sin(arctan)-ly. Used parameter values for plotting: $E_0 = 1$ eV, $\lambda/2\mu = 1/2$ eV, $b = 1$ m.

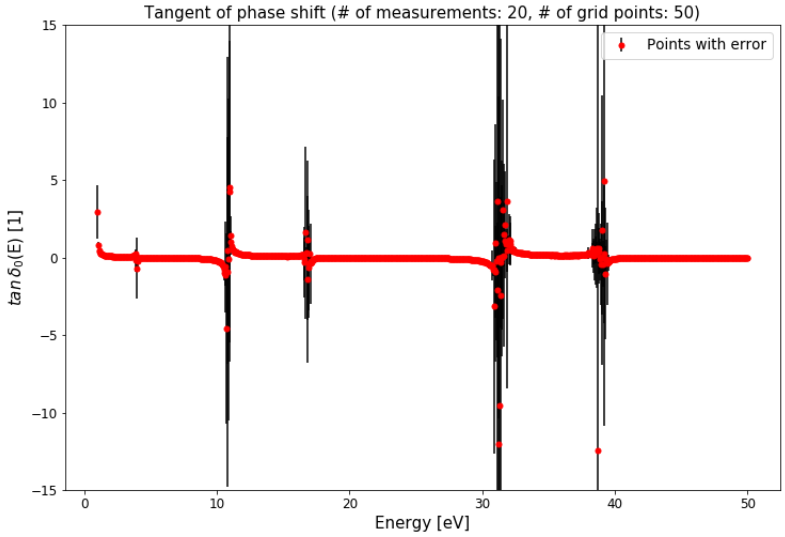

Figure 1: Tangent of the phase shift for the delta-shell potential.

Discussion

We can see that the diagonal matrix elements of R (as the function of E through k_0) and therefore $\tan\delta_0(E)$ and $\delta_0(E)$ show some kind of periodicity. We can see separated regions in energy within the mentioned quantities decreasing monotonely. The phase shift can be positive or negative, too, which is a really interesting and flabbergasting result.Near the borders, the errors get high. The cross section shows (resonance) peaks in some well-defined energy values, which are the same as the borders in the case of the previously examined quantities. Between them, the cross section is really small.

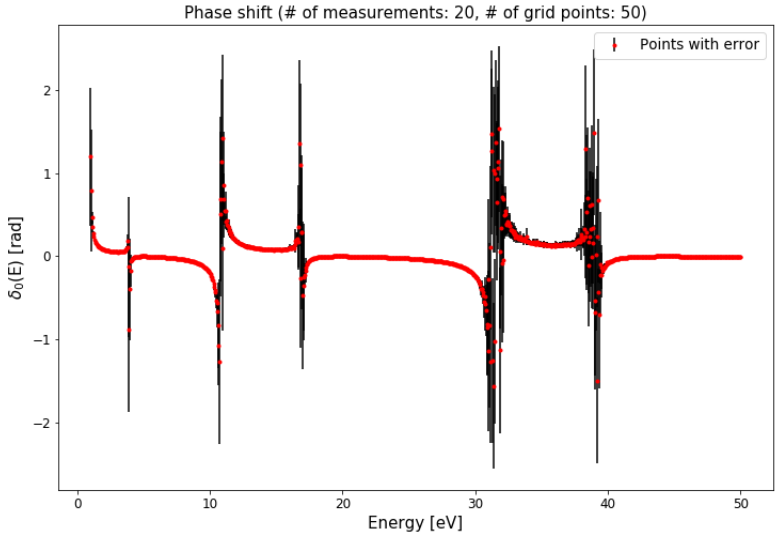

Figure 2: Phase shift for the delta-shell potential.

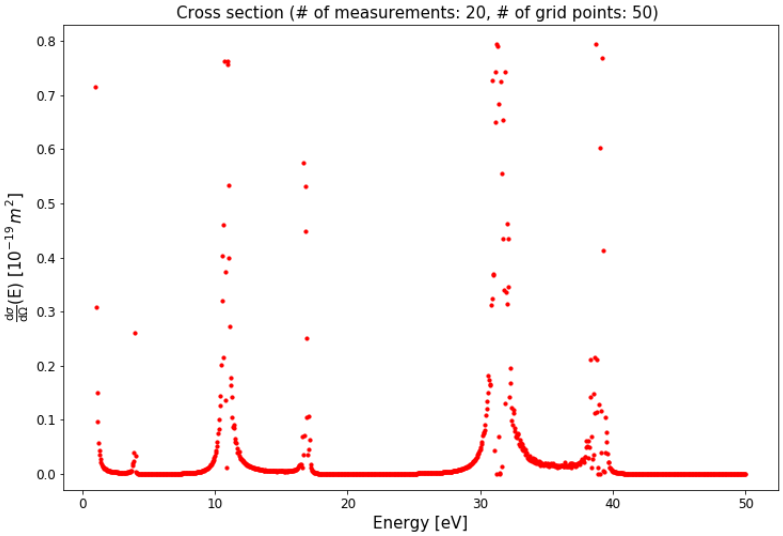

Figure 3: Cross section for the delta-shell potential.

B. $\cosh^{-2}(r)$ potential

$$\text{In coordinate space:} \quad V_{\cosh}(r) = a\cosh^{-2}(r-b). \tag{19}$$

We are furtunate because we can solve this potential analitically, but we don't get a result that can easily be interpreted qualitatively. In momentum space:

$$\begin{aligned}
V(k,p) &= -\frac{a}{kp}\int_0^\infty \mathrm{d}r\,\frac{\sin(kr)\sin(pr)}{\cosh^2(r-b)} \\
&= -\frac{a}{kp}\frac{\mathrm{e}^{2b}}{2(1+\mathrm{e}^{2b})}\Bigg\{ \\
&\quad -\frac{1}{-2i+k+p}\left[2i-k+p+(1+\mathrm{e}^{2b})(k-p)\times\ {}_2F_1(1,\frac{1}{2}i(-2i+k-p),\frac{1}{2}i(-4i+k-p);-\mathrm{e}^{2b}))\right] \\
&\quad +\ \frac{1}{2i+k-p}\left[2i+k-p-(1+\mathrm{e}^{2b})(k-p)\times\ {}_2F_1(1,-\frac{1}{2}i(2i+k-p),-\frac{1}{2}i(4i+k-p);-\mathrm{e}^{2b}))\right] \\
&\quad -\frac{1}{-2i+k+p}\left[2i+k+p-(1+\mathrm{e}^{2b})(k+p)\times\ {}_2F_1(1,\frac{1}{2}i(-2i+k+p),\frac{1}{2}i(-4i+k+p);-\mathrm{e}^{2b}))\right] \\
&\quad -\ \frac{1}{2i+k+p}\left[2i+k+p-(1+\mathrm{e}^{2b})(k+p)\times\ {}_2F_1(1,-\frac{1}{2}i(2i+k+p),-\frac{1}{2}i(4i+k+p);-\mathrm{e}^{2b}))\right]\Bigg\},
\end{aligned} \tag{20}$$

where the ${}_2F_1$ and i denotes the Hypergeometric function and the imaginary unit, respectively. If $b=0$, we get:

$$V(k,p) = \frac{a}{2kp}\left\{\frac{\pi}{2}(k+p)\sinh^{-1}\left[\frac{\pi}{2}(k+p)\right] - \frac{\pi}{2}(k-p)\sinh^{-1}\left[\frac{\pi}{2}(k-p)\right]\right\}. \tag{21}$$

For the sake of simplicity we only investigated this case, not the general one.

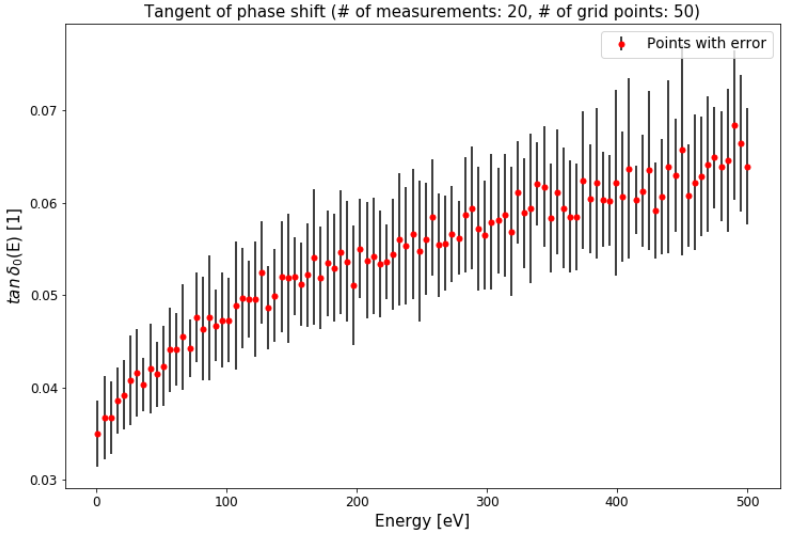

Figure 4: Tangent of the phase shift for the $\cosh^{-2}(r)$ potential.

We ran the simulation for one value of the parameters because we can easily guess the dependences from them. If a is increasing, V will so and therefore R and $\tan\delta_0$ in a linear way but the δ_0 will increase arctan-ly and $\mathrm{d}\sigma/\mathrm{d}\Omega$ sin(arctan)-ly. The value of b gives the place of the origin, so it is not relevant, therefore the result shouldn't depend on this quantity. Used parameter values for plotting: $E_0 = 1$ eV, $\mu = 1$ kg, $a = 1$ eV.

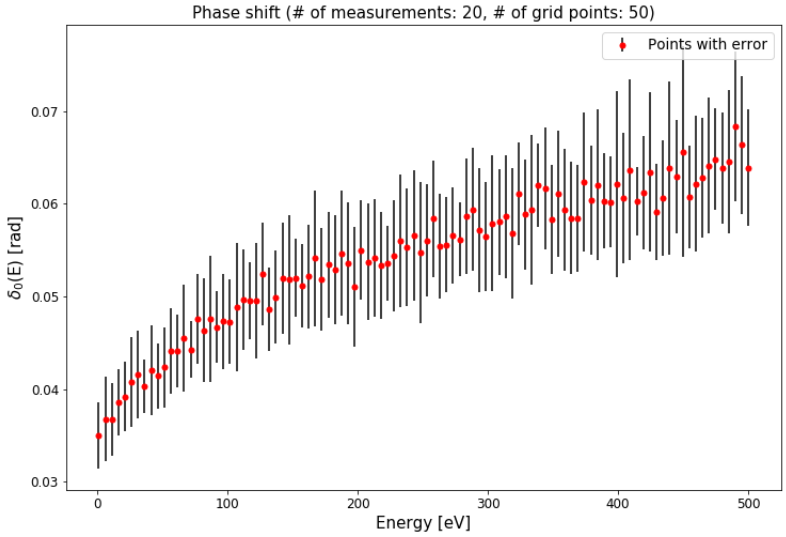

Figure 5: Phase shift for the $\cosh^{-2}(r)$ potential.

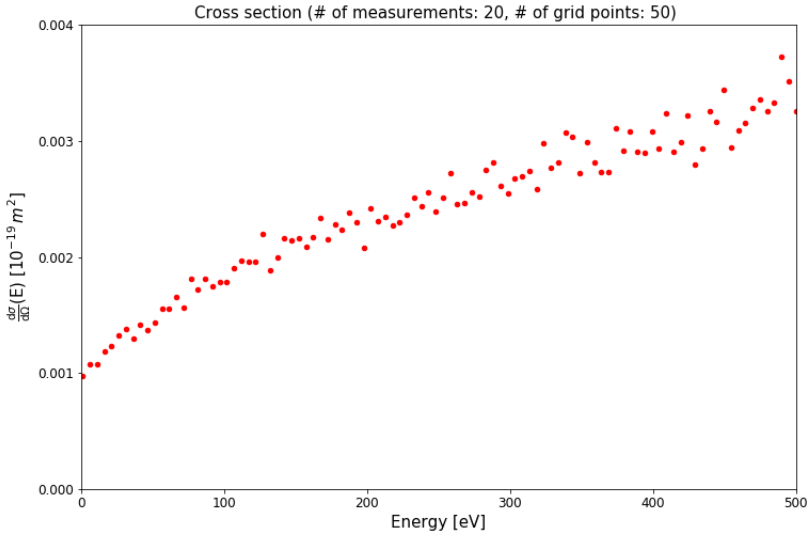

Figure 6: Cross section for the $\cosh^{-2}(r)$ potential.

Discussion

As opposed to the previous case, we do not see any kind of periodicity in the quantities' energy dependence. Rather, we can see that all the three quantities show increasing tendency with energy. The errors in this case are more uniform than what we experienced with the delta-shell potential. The order of magnitude of the phase space in this case is $\mathcal{O}(0.01$ rad), roughly tenth of the delta-shell's most frequent. We do not see resonances in the cross section plot.

C. Exponentially decaying potential

$$\text{In coordinate space:} \quad V_{\exp}(r) = a\mathrm{e}^{-br} \tag{22}$$

$$\text{In momentum space:} \quad V(k,p) = \frac{2ab}{(b^2+k^2)^2 + 2(b^2-k^2)p^2 + p^4} \tag{23}$$

If a is increasing, V will so and therefore R and $\tan\delta_0$ linearly, δ arctan-ly and σ sin(arctan)-ly. To see the b-dependence we present 3 different cases below for $b = 0.5$, $b = 4$ and finally $b = 2$.

The $b = 0.5$ case

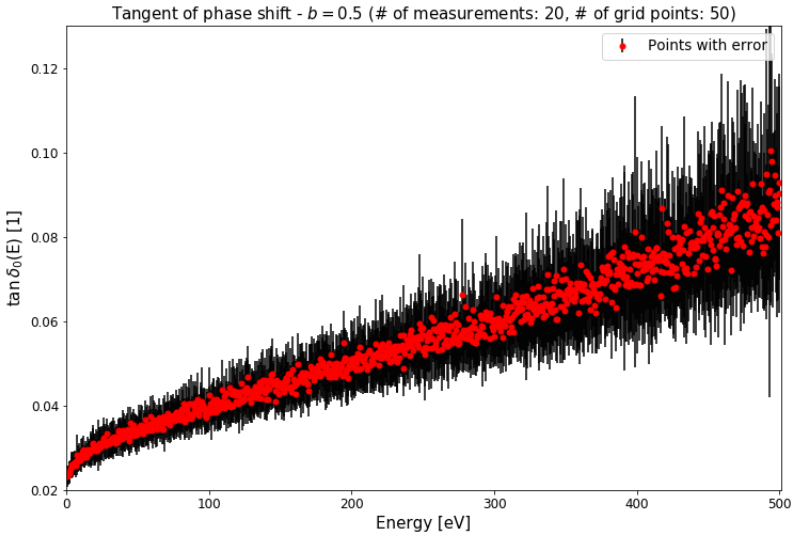

Figure 7: Tangent of the phase shift for the exponentially decaying potential for $b = 0.5$.

Discussion

We can see increasing tendency in each quantity with energy. This tendency is not linear. It can be seen that not just the quantities but the errors are increasing with the energy, too. These errors are less uniform than the previous case. The phase shift is positive. The order of magnitude of the cross section is the same that the experienced at the $\cosh^{-2}(r)$ potential.

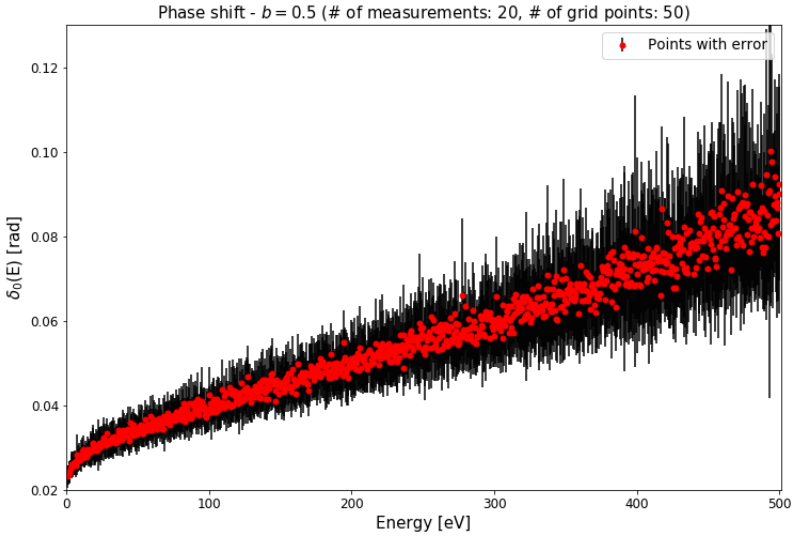

Figure 8: Phase shift for the exponentially decaying potential for $b = 0.5$.

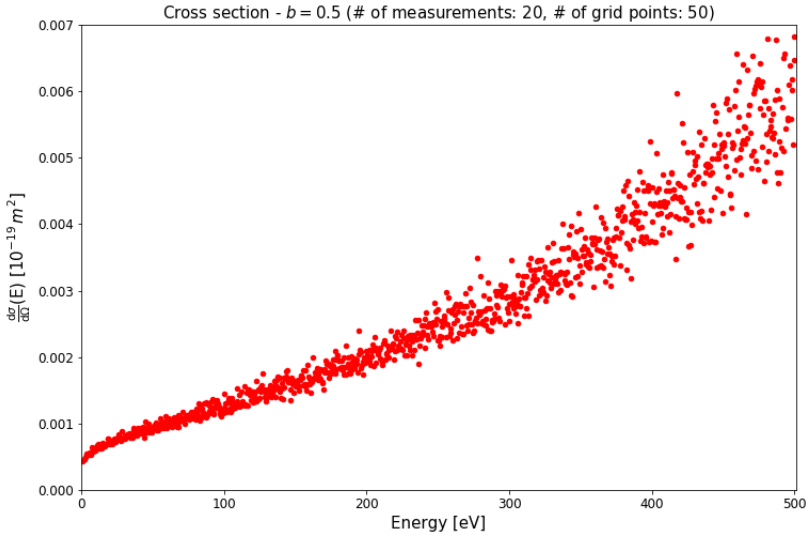

Figure 9: Cross section for the exponentially decaying potential for $b = 0.5$.

The $b = 4$ case

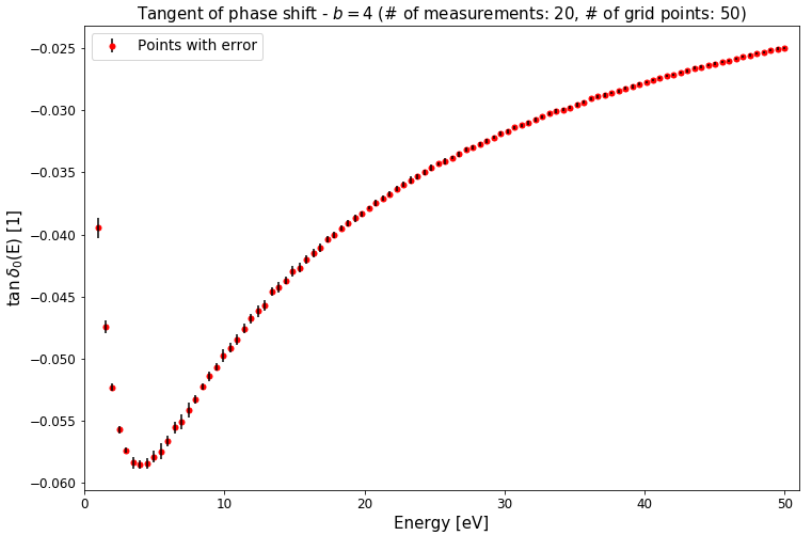

Figure 10: Tangent of the phase shift for the exponentially decaying potential for $b = 4$.

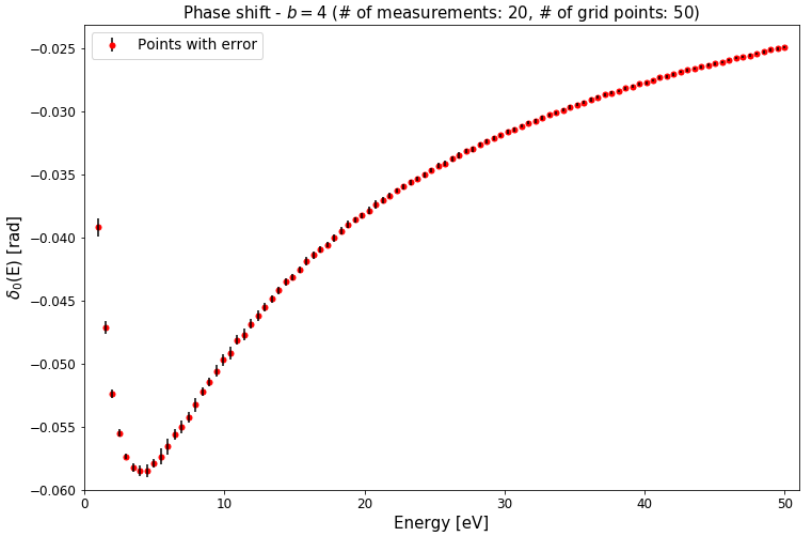

Figure 11: Phase shift for the exponentially decaying potential for $b = 4$.

Discussion

The $\tan\delta_0$, therefore the reaction amplitude and the phase shift show interesting energy dependence, namely they have a minimum point at around 4 eV. The phase shift is negative in this case. The errors are significantly lower than in the

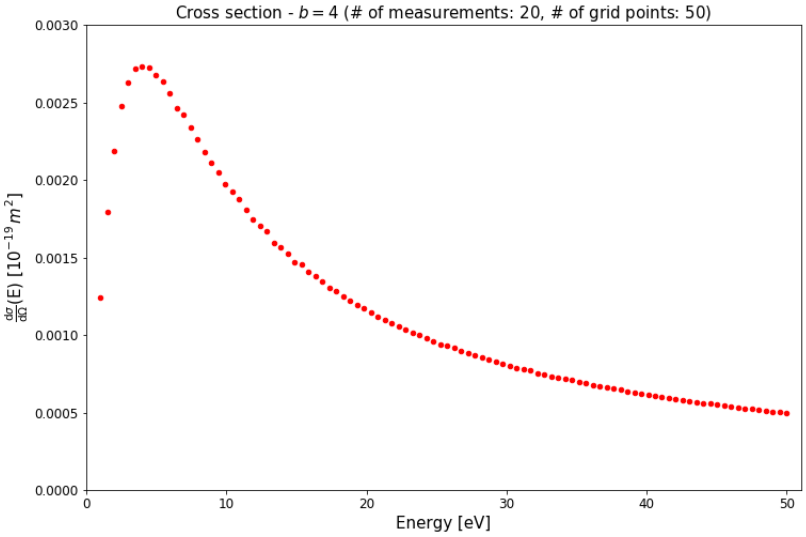

Figure 12: Cross section for the exponentially decaying potential for $b = 4$.

$b = 0.5$ case. The order of magnitude of the cross section is the same that the experienced at the $\cosh^{-2}(r)$ potential and the $b = 0.5$ case, but it has a resonance peak around 4 eV which has roughly 3 times higher in order of magnitude.

The $b = 2$ case

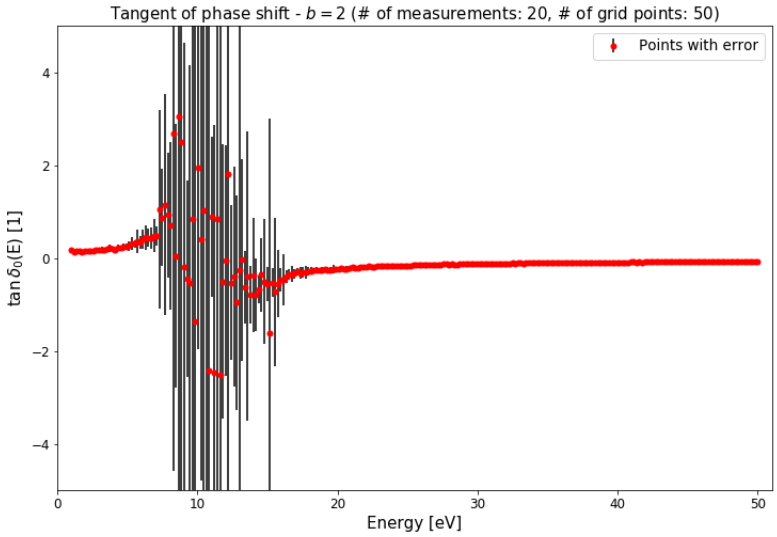

Figure 13: Tangent of the phase shift for the exponentially decaying potential for $b = 2$.

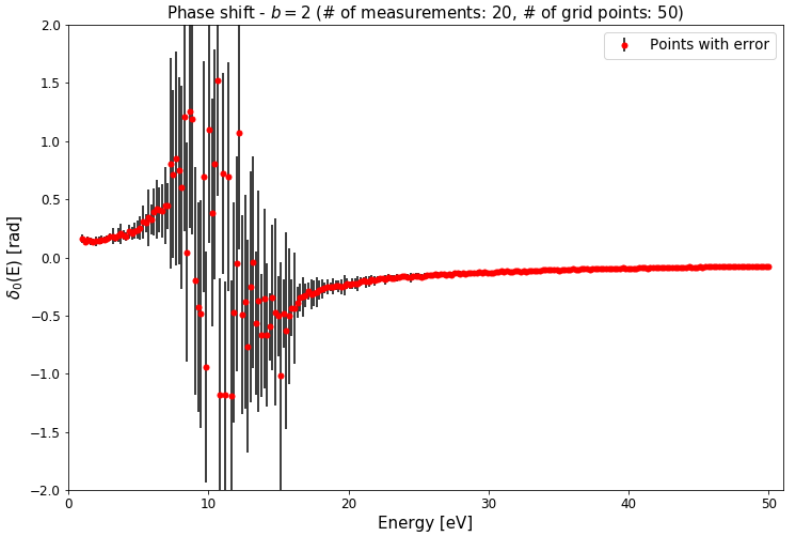

Figure 14: Phase shift for the exponentially decaying potential for $b = 2$.

Discussion

We think the $b = 2$ case must be in the context, too, because we can get some additional information about Python's Gauss elimination rutin. It is obvious that there are some "problem" in the 7-15 eV energy range, because we can only see

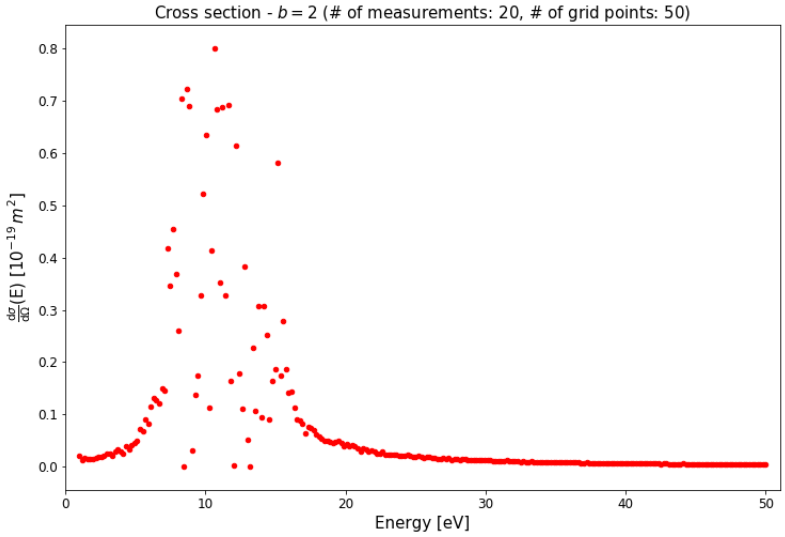

Figure 15: Cross section for the exponentially decaying potential for $b = 2$.

mess on every function in this interval. We tried to run the simulation using fewer or more points and calculating only in the 5-20 eV, but nothing solved our problem, in each case we found ourselves in this kind of situation. But what we can learn from it? For answering the question we need to think about how one point (and the corresponding error) generates. For a given energy value we use 20 different weighting and average them. We have 50 grid points in momentum space, therefore the (8) is a 51 dimensional linear equation system. We solve it with Gauss elimination, which means roughly $2 \cdot 51^2 \approx 5000$ operation for one weighting. This means that for one single point we have to take ~ 100.000 operations, it is a huge number. Numerical error can be generated in each step because the finite precision (finite number of digits are stored) of the Python's corresponding package. This can result the incomprehensible behaviour of the quantities on the plots above. Conclusion: instead of this Python package one should use another, more sophicticated one for computation that requires huge amount of steps.

D. Gaussian potential

$$\text{In coordinate space:} \quad V_{\text{Gauss}}(r) = a\mathrm{e}^{-b(r-c)^2} \tag{24}$$

$$\text{In momentum space:} \quad V(k,p) = \frac{a}{4}\sqrt{\frac{\pi}{b}}\left[\mathrm{e}^{-(k-p)^2/4b} - \mathrm{e}^{-(k+p)^2/4b}\right] \tag{25}$$

If a is increasing, V will so and therefore R and $\tan\delta_0$ linearly, δ_0 arctan-ly and $\mathrm{d}\sigma/\mathrm{d}\Omega$ sin(arctan)-ly. For general c we did not get the momentum space formula from Mathematica, therefore we only study the $c = 0$ case what momentum space potential form can be shown above. To see the b-dependence we present 2 different cases below for $b = 1$ and $b = 4$.

The $b = 1$ case

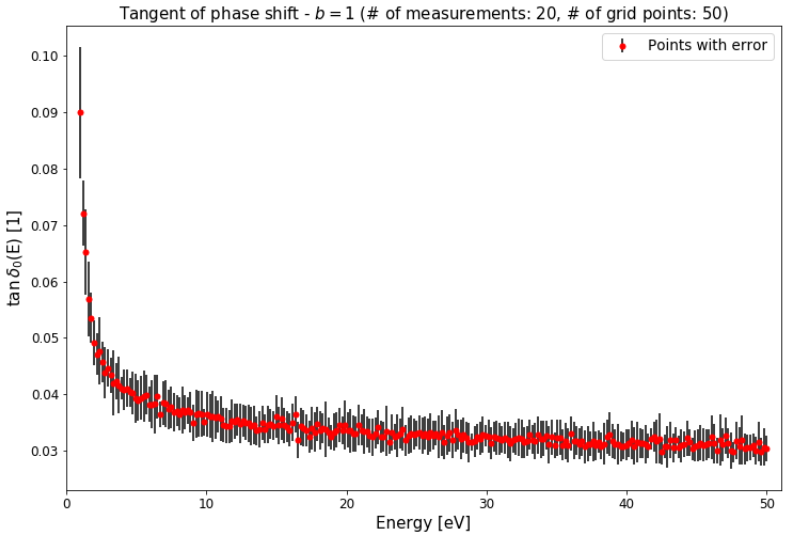

Figure 16: Tangent of the phase shift for the Gaussian potential for $b = 1$.

Discussion

The tangent of the phase shift and itself are decreasing rapidly, and parallel to this the error is also decreasing but from $\sim 5-10$ eV the error's magnitude does not change. We plotted the phase shift in a logarithm scale in Figure 18. The plot shows us that the decreasing is so rapid, that in the logarithmic scale we can see harder decreasing than the linear, what it means is the decreasing of the phase shift as a function of energy decreases more rapid than exponential. It means, that in higher energies the particles feel almost no scattering potential. The cross section is decreasing extremely rapid, too.

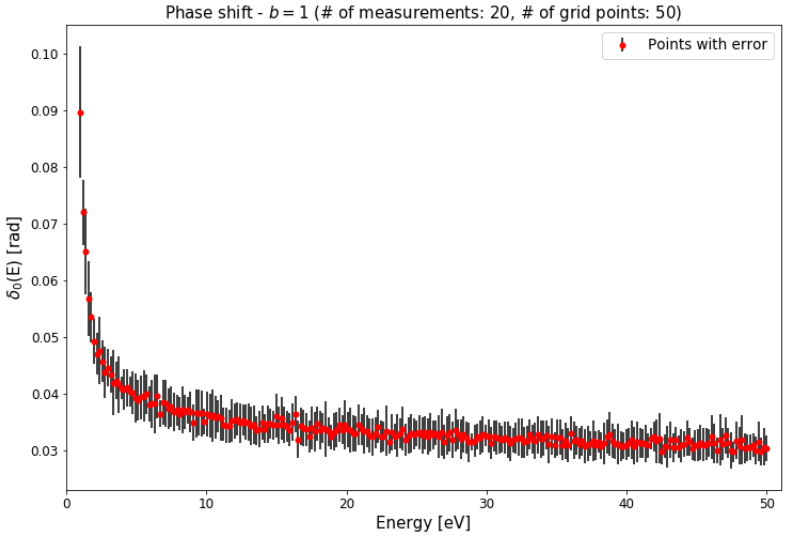

Figure 17: Phase shift for the Gaussian potential for $b = 1$.

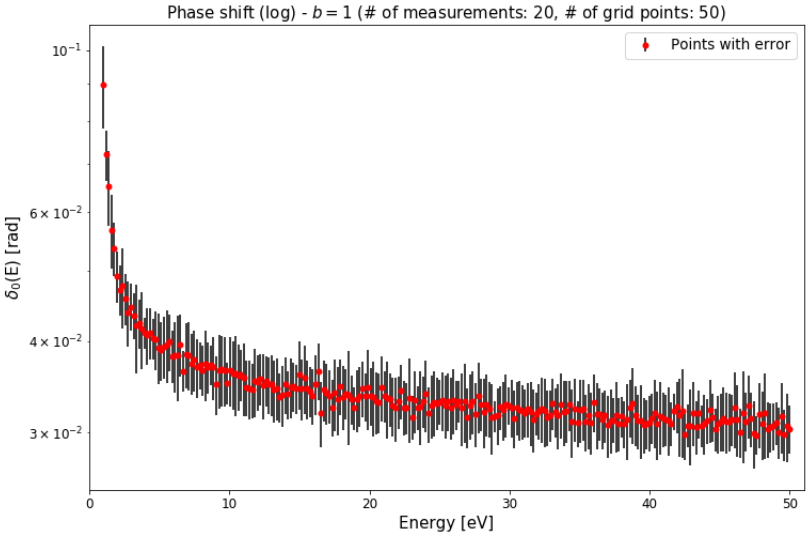

Figure 18: Phase shift in a logarithmic scale for the Gaussian potential for $b = 1$.

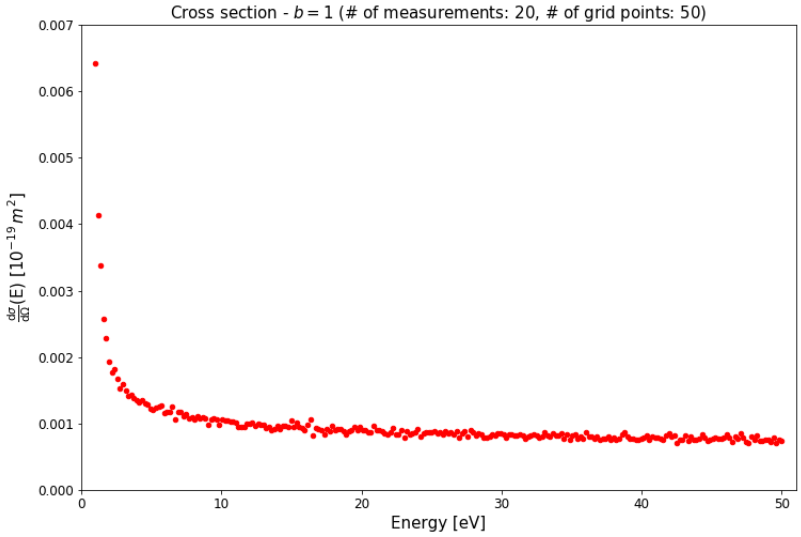

Figure 19: Cross section for the Gaussian potential for $b = 1$.

The $b = 4$ case

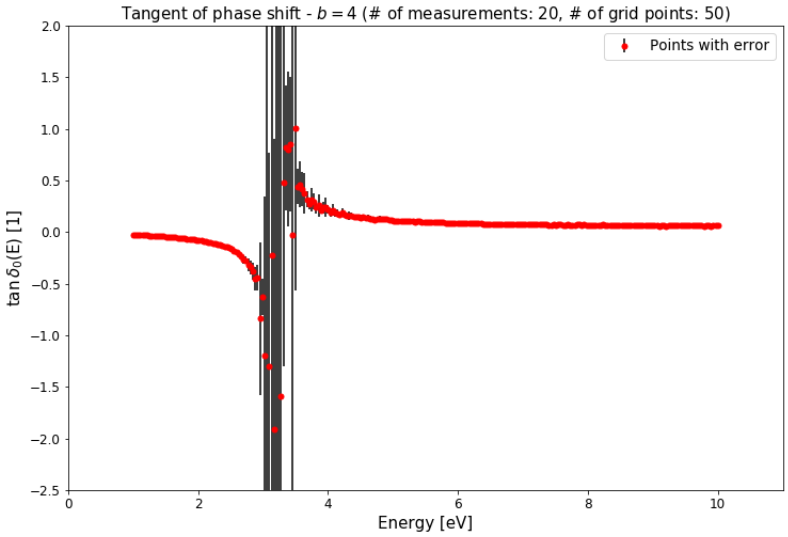

Figure 20: Tangent of the phase shift for the Gaussian potential for $b = 4$.

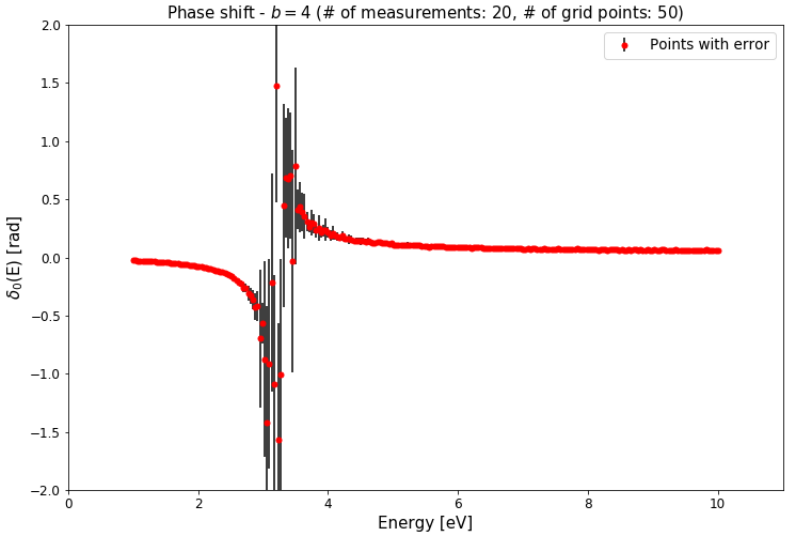

Figure 21: Phase shift for the Gaussian potential for $b = 4$.

Discussion

We can see a similar problem in here to the $b = 2$ case in the exponentially decreasing scenario, but here the incoordination is not so big than the other case. We can see a critical section in ~ 3 eV, where the errors are really high with respect

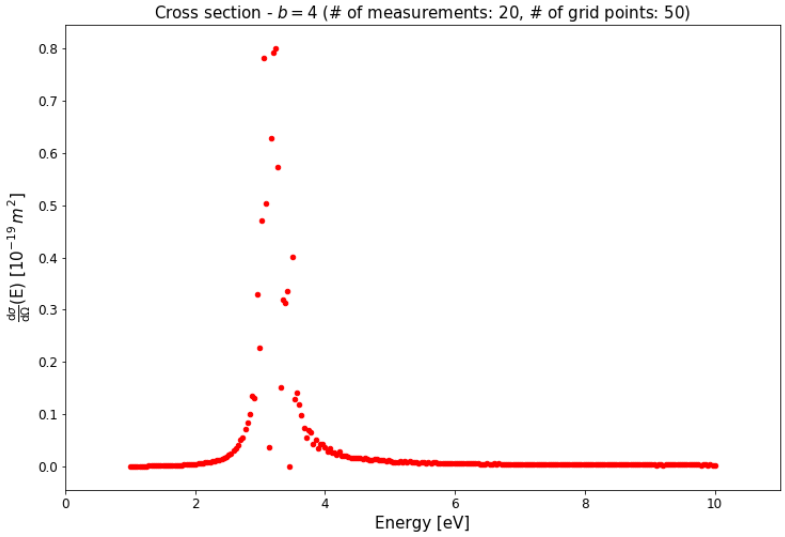

Figure 22: Phase shift for the Gaussian potential for $b = 4$.

to the values and the other errors, too. and the phase shift swap the sign here. More precisely, it looks from the tangent of phase shift picture that this quantity diverges, so the phase shift diverges, too. (For confirm this statement, detailed analitical calculations needed.) The cross section has a peak at this energy value, but the incoordination is present here also.

E. Yukawa potential

$$\text{In coordinate space:} \quad V_{\text{Yukawa}}(r) = a\frac{\mathrm{e}^{-br}}{r} \tag{26}$$

$$\text{In momentum space:} \quad V(k,p) = \frac{a}{4kp}\log\left[\frac{(k+p)^2+b^2}{(k-p)^2+b^2}\right] \tag{27}$$

If a is increasing, V will so and therefore R and $\tan\delta_0$ linearly, δ_0 arctan-ly and $\mathrm{d}\sigma/\mathrm{d}\Omega$ sin(arctan)-ly. To see the b-dependence we present 2 different cases below for $b = 1$ and $b = 4$.

The $b = 1$ case

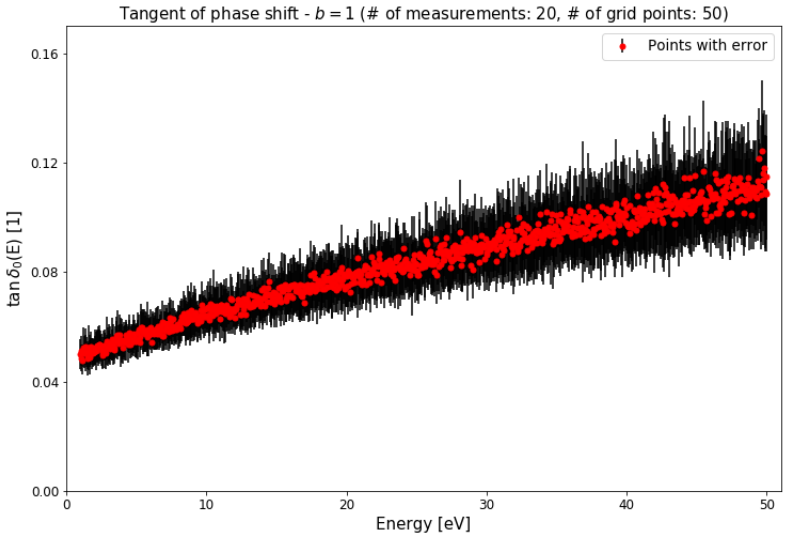

Figure 23: Tangent of the phase shift for the Yukawa potential for $b = 1$.

Discussion

The results are really similar to the exponentially decaying case. It it quite intuitive, because the Yukawa potential is an exponentially decaying potential divided by the distance, and the exponential functions are much more powerful than the polinomials. We can see increasing tendency in each quantity with energy. This tendency is not linear, but a linear fit would not too far from the truth, especially for the cross section. It can be seen that not just the quantities but the errors are increasing with the energy, too. These errors are less uniform than the $\cosh^{-2}(r)$ case. The phase shift is positive. The order of magnitude of the cross section is the same that the experienced at the $\cosh^{-2}(r)$ and the exponentially decaying potential.

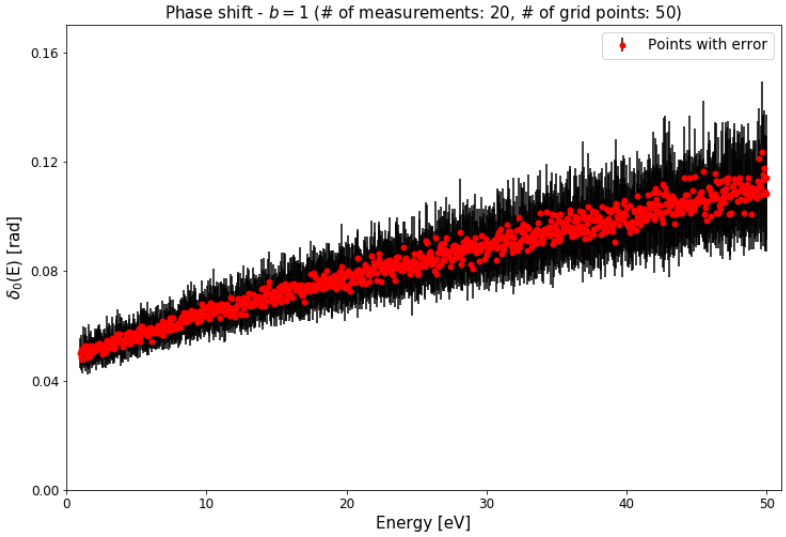

Figure 24: Phase shift for the Yukawa potential for $b = 1$.

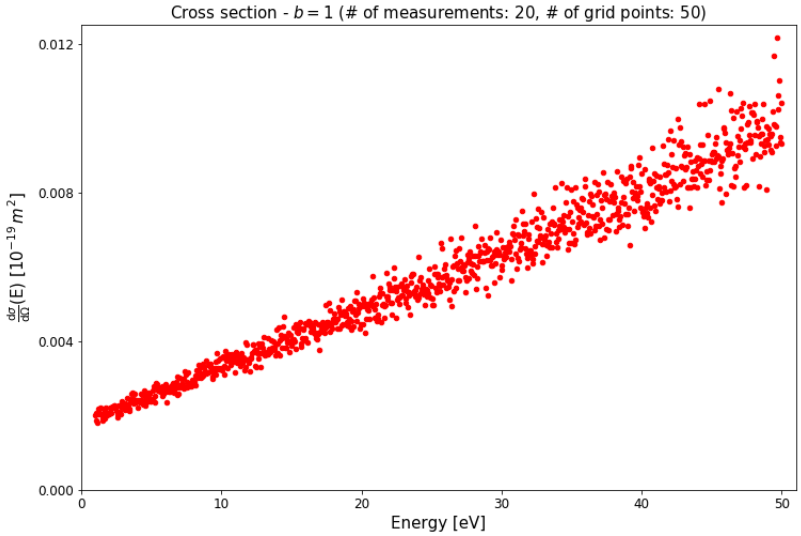

Figure 25: Cross section for the Yukawa potential for $b = 1$.

The $b = 4$ case

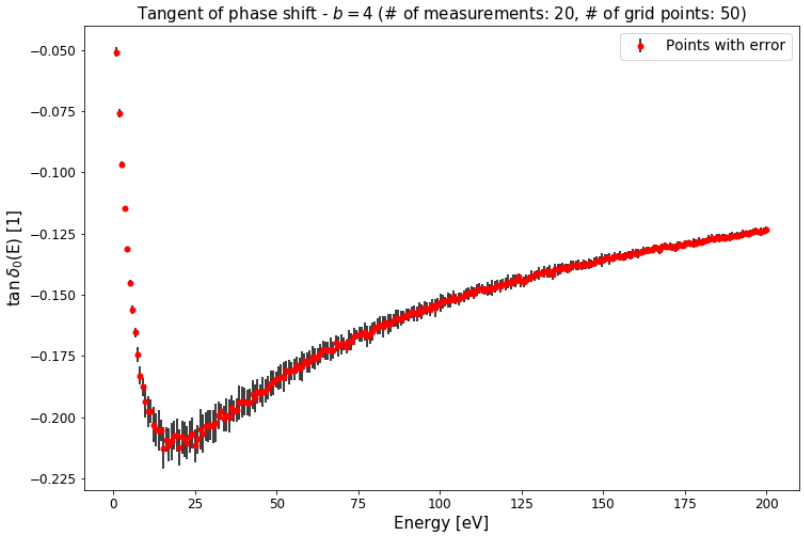

Figure 26: Tangent of the phase shift for the Yukawa potential for $b = 4$.

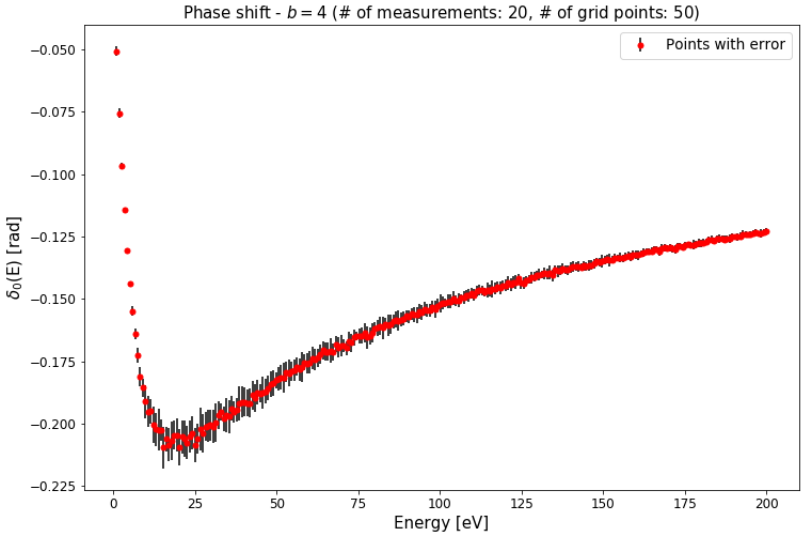

Figure 27: Phase shift for the Yukawa potential for $b = 4$.

Discussion

The $\tan\delta_0$, therefore the reaction amplitude and the phase shift show interesting energy dependence, namely they have a minimum point at around 20 eV. The phase shift is negative in this case. The errors are significantly lower than in

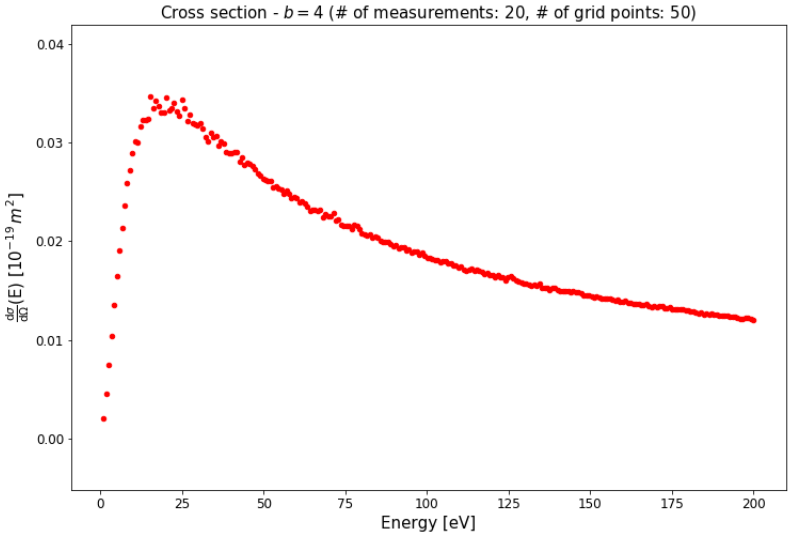

Figure 28: Cross section for the Yukawa potential for $b = 4$.

the $b = 1$ case, but higher than the $b = 4$ exponential case. The order of magnitude of the cross section is 1 order of magnitude higher than the $b = 4$ exponential case, it is caused by the extra polinomial. The cross section has a resonance peak around 20 eV.

IV. SUMMARY

In this project we discussed the Lippmann-Schwinger equation and its properties for various potentials in a numerical way. After discretizing the equation we were able to solve it numerically as a linear equation system. With the help of Wolfram Mathematica we were able to calculate the momentum-space form of the potentials, which we used for the solution. We tried to give a broader analysis of this theorem, namely we investigated the phase shift and the cross section given by the $l = 0$ sector approximation of the partial wave analysis.

Our results can be seen on the figures, where we plotted the phase shift, its tangent and the cross section as a function of the initial center of mass energy. We were able to see resonances in the cross section curves and examples for the phase shift with positive and negative values, too.

The order of magnitude of the resonance peaks are not the same but can be put to two categories, wherein the magnitudes are almost the same. The difference between these two categories is a factor of ~ 30.

We were able to detect incoordination in some phase shifts. In the first case we came to the conclusion that the Gauss elimination algorithm should be more precise for excercises that require this amount of operations. In the second case, we detect a "singularity" in the phase shift.

Remarks. Unfortunately, we were not taken into account the correct order of magnitudes of the parameter values. For example, our plots show the results with $\mu = 1$ kg and $b = 1$ m for the delta-shell potential and $b = (0.5 - 4)$ 1/m for the other potentials. They are quite wrong values if we want to compare our numerical results for the experimental data but they have no effect on the shape of the functions, just on the order of magnitudes. Unfortunately, we did not have capacity to run the simulations and calculate the quantities again, therefore this project report contains the semi-real input parameters and results. But we want to emphasize that the order of magnitude probably does not effect the shapes significantly. (If we want to describe a nucleon-nucleon scattering, we have to use $\mu \approx m_{nucleon}/2 \approx 470$ MeV and $b \approx 10^{15}$ 1/m. For seismic processes μ will be much higher and b will be much lower than in the nucleonic case.)

We want to have another remark here, that probably all the potentials provide at least resonance peak in the cross section curve but the reason that we did not see them is that they are out of the examined energy range. So, with this comment we can refine our discussions in a way that all of the mentioned statements and conclusions hold for the examined energy interval.

In our opinion, for the outlook it would be an interesting task to study a theory with taking into account partial waves with higher l values.

References

[1] `https://en.wikipedia.org/wiki/Lippmann%E2%80%93Schwinger_equation`

[2] Landau, Rubin H., Manuel J. Páez, and Cristian C. Bordeianu. *Computational physics: Problem solving with Python.* John Wiley & Sons, 2015.